Damping of Water Hammer with Cavitation in Rocket Engine Feed Lines

By Sebastian KLEIN,[1)] Tobias TRAUDT,[1)] Cristiano BOMBARDIERI,[2)] and Michael OSCHWALD[1)]

[1)]*Institute of Space Propulsion, DLR, Lampoldshausen, Germany*
[2)]*ArianeGroup, Bremen, Germany*

(Received June 21st, 2019)

Water hammer phenomena are of great interest in the field of rocket engineering. Closing a valve rapidly to shut down a rocket engine or stop the chill down procedure can lead to water hammer in the piping system. These high amplitude pressure oscillations can damage the components of the engine. If the vapour pressure is undercut, cavitation will occur. Water hammer damping experiments, some with and some without the occurrence of cavitation, have been performed at the **F**luid **T**ransient **T**est **F**acility (FTTF) at DLR Lampoldshausen. The main aspect of interest in this paper is the influences of the cavitation on the damping of the pressure oscillation. Therefore tests with and without cavitation will be compared to isolate the impact of the cavitation.

Key Words: Water hammer, Two-phase flow, cavitation, damping, rocket engine

Nomenclature

c	:	speed of sound, m/s
d	:	diameter, mm
e	:	wall thickness, mm
E	:	modulus of elasticity, N/m^2
f	:	frequency, Hz
K	:	compressibility, N/m^2
l	:	length, m
M	:	Mode
$\dot{m}$	:	mass flow, kg/s
P	:	pressure, bar
t	:	time, s
v	:	flow velocity, m/s
y	:	damping function
δ	:	damping coefficient
ν	:	Poisson's ratio
ρ	:	density, kg/m^2
ϕ	:	phase shift, 1/s
ω	:	angular frequency, 1/s
Subscripts		
h	:	harmonic oscillation
HP	:	high pressure tank
LP	:	low pressure tank
i	:	number of valleys
n	:	number of peak

1. Introduction

The water hammer phenomenon leads to high pressure peaks, these pressure peaks are a critical design parameter for rocket engines feedline systems. Due to the stopping of a fluid flow by a rapid closing valve a pressure wave is travelling upstream the pipeline. This pressure wave leads to pressure peaks around 220 to 230 bar in the ATV spacecraft system. A re-priming network was added to get rid of these high pressures.[1)]

In the Atlas 2 rocket three engines in the main stage are used, two booster engines at the side and one sustainer engine in the center. Before separation of the side engines the LOX-line valve is closed as described by Walter et al. in Ref. 2). This valve closure triggers a water hammer in a variable-g environment. The comparisson of simulation and flight data showed good agreement as shown by Walker in Ref. 3).

A well known case is the loss of the N1 rocket at its 4th flight. The shock after shutdown of the six central engines caused the destruction of an oxygen pump.[4)]

Investigation of water hammer is done scientifically since the late 19th century. The work of Joukowsky is one of the basics in this field, he described the pressure rise after valve closure. An overview about research activities is given by Bergant et al. in Ref, 5) and by Ghidaoui et al. in Ref. 6). A very detailed overview into the cavitation research in the twentieth century written by Bergant et al. can be found in Ref. 7). Most of these investigations were performed with water.

For rocket propulsion investigations with real propellant and cryogenic fluids are of great interest Tests with Mono Methyl Hydrazine and Nitrogen Tetroxide have been performed by Gibek et al in Ref. 8).. On the cryogenic side priming tests with liquid Nitrogen were performed and compared to numerical simulations by Gouriet et al.[9)]

Several water hammer tests with and without cavitation have been performed at the FTTF at DLR Lampoldshausen by Traudt et al.[10,11)] The water hammer was created by using a fast closing valve to stop a steady flow. Traudt et al. showed in Ref. 11) tests in which the 2nd peak is up to 25% higher than the 1st peak. They used an optical access to investigate occurring cavitation phenomena. A method to track cavitation bubbles in the flow was presented. Intermediate spikes were found in the cavitation time range, the first spike is accompanied by reversal of the flow direction.

Priming tests with cavitation at the same test bench done by Bombardieri showed that the damping behaviour changes depending on the static pressure.[12)] The same dependence was observed in water hammer tests. For lower static pressures in the system higher damping constants have been identified by Klein et al. in Ref. 13) but could not been explained.

In this paper the influence of the cavitation will be investigated. Therefore water hammer tests at a static pressure range from $p = 2 - 45$ bar, all with cavitation, will be compared with the experiments from Ref. 13). In total 71 experiments with

Table 1. Dimensions of the test bench.

Description	Symbol	Value
Test section length	l_{ts}	7.671 m
Test section inner pipe diameter	$d_{i,ts}$	19 mm
Test section wall thickness	e_{ts}	1.5 mm
Sensor 1 distance from valve seat	l_1	0.3 m
Sensor 2 distance from valve seat	l_2	6.9 m
Sensor 3 distance from valve seat	l_3	7.6 m

and 29 experiments without cavitation are part of this study.

2. Test bench

The **F**ast **T**ransient **T**est **F**acility (FTTF) at DLR Lampoldshausen consists of two pressurized tanks, a test pipeline, a coriolis flow meter and a fast closing axial valve.

A schematic overview is given in Fig. 1, the CAD model of the test bench is shown in Fig. 2. Two tanks (1,2) are connected with a test pipe (3). A fast closing coaxial valve (4) and a Coriolis flow meter are mounted between the low pressure tank (2) and the test pipe (3). Both tanks are pressurized with gaseous nitrogen. By varying the pressure difference between the high pressure tank P_{HP} and the low pressure tank P_{LP} the fluid can be pumped from one tank to the other. Due to regulation the accuracy of the tank pressures P_{HP} and P_{LP} is within ±0.4%.

The tanks and the test section are made of stainless steel of grade 1.4541. The closing time of the valve is around $t_{valve} = 18 \pm 2$ ms. The test pipe is a one and a half spin spiral with a diameer of 1.25 m and an upward slope of $\sim 1°$. Three sensor positions are used along the pipe. A static pressure sensor (Kistler 4043A - 100) with a sampling rate of $f_{stat} = 10$ kHz and a dynamic pressure sensor (Kistler 601A) with a sampling rate of $f_{dyn} = 150$ kHz are present at each sensor position. The sensor positions and other important geometry parameters are summarized in table 1.

More detailed information about the test bench and test activities at the FTTF can be found in Refs 10, 11, 13).

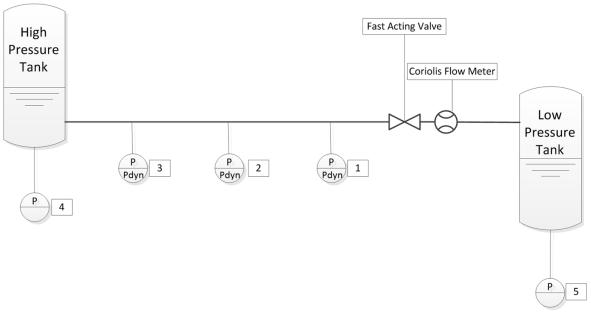

Fig. 1. Schematic overview of the FTTF[13)]

2.1. Test procedure

The test bench is filled with water which is stored overnight to remove any undissolved gas. By pressurizing the tanks a stationary flow in the pipeline from the high pressure tank (1) to the low pressure tank (2) is created. The axial valve (4) is closed, this leads to a water hammer event up- and downstream of the valve. This pressure surge is detected at the three sensor rings in the test section (3).

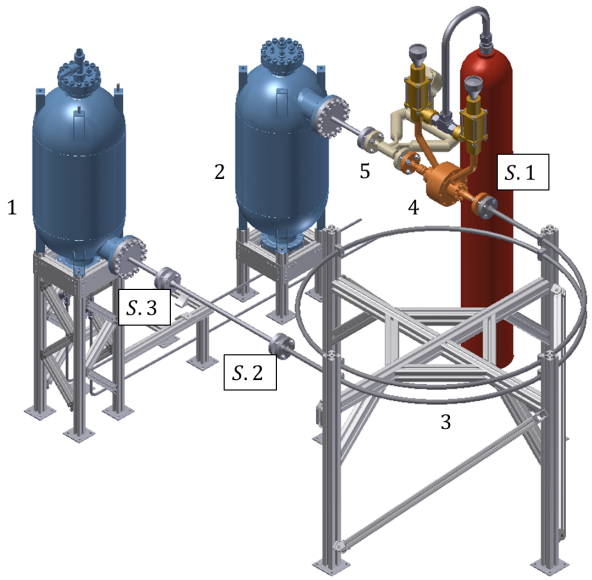

Fig. 2. CAD model of the FTTF: High pressure tank [HP] (1), low pressure tank [LP] (2), test pipe (3), fast closing axial valve with pressurization system (4), Coriolis flow meter (5), sensor rings (S.1 - S.3)[13)]

3. Theoretical Background

The Joukowsky equation is one of the fundamental equations for water hammer. It is valid for an instantaneous change in speed, therefore an instantaneous closing valve. The pressure rise ΔP is the product of the density ρ, the speed of sound c and the change of velocity Δv.

$$\Delta P = \rho c \Delta v \tag{1}$$

The pressure wave induced by the fast closing valve travels upward the pipeline with the speed of sound c. An analytical correlation is used to estimate the speed of sound in the fluid.[14)]

$$c^2 = \frac{\frac{K}{\rho}}{1 + \left[\left(\frac{K}{E}\right)\left(\frac{d}{e}\right)\right] c_1} \tag{2}$$

Where K is the compressibility, ρ the density, E the modulus of elasticity, d and e are the length and wall thickness of the pipe. Since the ratio of length and wall thickness $d/e = 12.7$ the correction factor c_1 is calculated by the following equation for a thick walled pipe.[14)]

$$c_1 = \frac{2e}{d}(1 + \nu) + \frac{d(1 + \nu^2)}{d + e} \tag{3}$$

The Poisson coefficient is called ν. For this test bench at room temperature at ambient pressure with no gas in the test section the speed of sound $c = 1392$ m/s as calculated by Traudt et al. in Ref. 10).

The speed of sound changes dramatically with the occurrence of cavitation. The speed of sound in a two-phase flow has been described by Wilson et al.[15)]

The eigenfrequency f is calculated with $f = c/4l$, where l is the length of the pipe.

To determine the damping of the oscillation the well known damping function

$$y(t) = \hat{y} e^{-\delta t} \tag{4}$$

is used, where $\hat{y}$ is the first (and highest) peak and ρ is the damping constant. The function $y(t)$ is fitted to the peaks of the pressure signal since an exponential damping behaviour is assumed.

An exponential damped oscillating pressure signal can be decomposed into its modes M_n with $n \in \mathbb{N}$. The first two modes can be described with Eqs. 5 and 6, where ω_i is the angular frequency. A shift in time of the whole signal can be realized by the phase shift ϕ_i.

$$M_1 = sin(\omega_1 \cdot t + \phi_1)\hat{y} \cdot e^{-\delta_1 t} \tag{5}$$

$$M_2 = sin(\omega_2 \cdot t + \phi_2)\hat{y} \cdot e^{-\delta_2 t} \tag{6}$$

4. Results

In this chapter the results of 100 test runs will be evaluated. First the test cases with- and without cavitation will be studied separately.

4.1. Declaration

To discuss the results an uniform nomenclature is mandatory. The declaration used in this paper is shown in Fig. 3. A schematic/typical test case with cavitation is shown.

The oscillation of the pressure is around the pressure in the high pressure tank P_{HP}. All local pressure peaks P_n are counted by $n \in \mathbb{N}$. The pressure peaks $\Delta P_n = P_n - P_{HP}$ are the differences to the pressure in the HP tank. The time difference between two peaks is given by $\Delta t_{i,i+1}$ with $n \in \mathbb{N}$. These time intervals differ for test cases with the occurrence of cavitation, if there is no cavitation, they are of equal length.

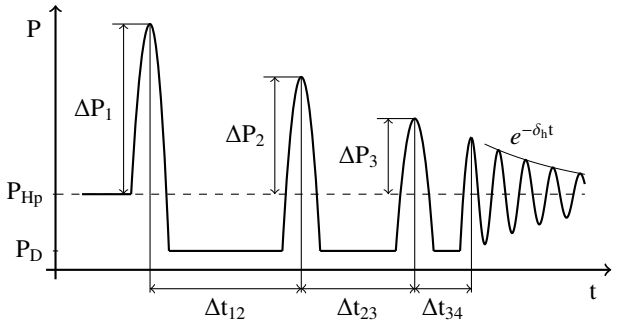

Fig. 3. Declaration

4.2. Test cases

In Fig. 4 the static pressure P_{HP} and the maximum pressure peak P_{max} for all test cases are shown. The pressure values which belong together are directly above each other. P_{HP} ranges from $2 - 43$ bar. By varying the pressure difference between both tanks the flow velocity v in the pipeline can be changed. With respect to Eq. 1, this leads to a varying P_{max}. Several tests with similar P_{HP} and P_{max} have been performed to ensure reproducibility.

The occurrence of cavitation depends on the relative maximum peak pressure P_{max}/P_{HP}. For most cases the maximum pressure is at the first peak ΔP_1. In some cases beat coupling happens, here the second peak can be higher than the first one. The maximum relative peaks P_{max}/P_{HP} for all test cases (sorted by P_{HP} are shown in Fig. 5. Since the pressure wave oscillates around the tank pressure p_{HP} with the maximum amplitude $P_{max} - P_{HP}$, occurrence of cavitation is possible

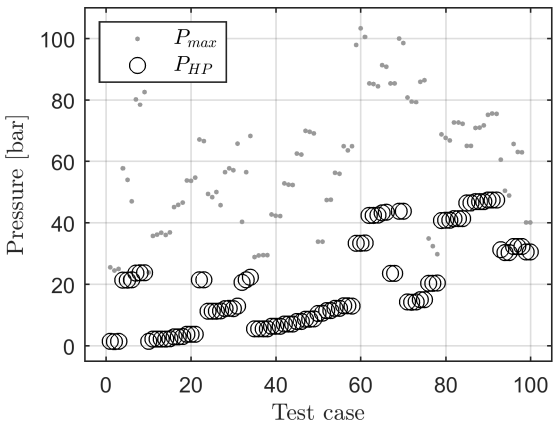

Fig. 4. Static pressure P_{HP} and maximum pressure P_{max} for all test cases.

if $P_{max}/P_{HP} > 2$. Tests at a constant P_{HP} have been performed with different relative amplitudes. Only at low tank pressures high relative amplitudes were reached. As seen in figure 4 the maximum pressure at the FTTF is around $p = 100$ bar. For test cases at $p_{HP} = 45$ bar, this leads to a relative amplitude of 2.2.

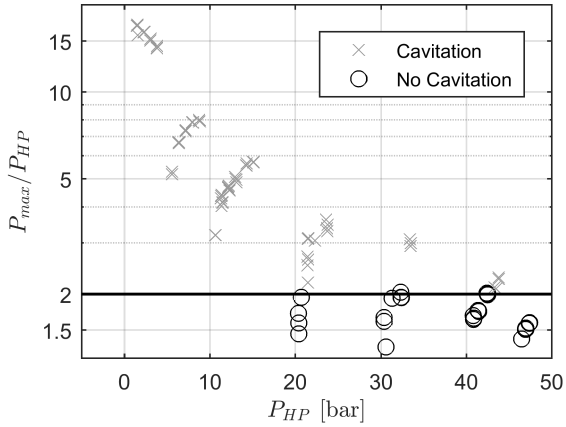

Fig. 5. Relative maximum presure P_{max}/P_{HP} for all test cases.

Three of these test cases will be treated in detail. The pressure signals at position 1 are shown in Fig. 6.

- Case **A** (top) is a water hammer without the occurrence of cavitation. Overtones are visible in the first ~ 10 peaks.
- Case **B** (middle) is a water hammer test with occurrence of cavitation in the first 6 wave troughs.
- Case **C** (bottom) is a water hammer test case with the occurrence of cavitation at the first wave trough. This case is considered to be the border case between case A and B.

4.3. Frequency Analysis

To identify the frequencies of the overtones a sliding FFT is used. The window width is $\Delta t_{width} = 200$ ms while the window progress is $\Delta t_{progress} = 40$ ms.

Case A

In figure 7 the pressure trace and FFT of windows 1 and 5 are shown. Window 1 is from $t = 4600 - 4800$ s, while window 5 is $t = 4761 - 4961$ ms. The main oscillation is at $f = 45$ Hz while the 2nd mode is at $f = 130$ Hz. Both FFTs are showing the same frequencies for both modes. Since the geometry is constant this is the expected behaviour. The test pipe can be considered a $\lambda/4$ resonator, therefore it is expected that the 2nd mode

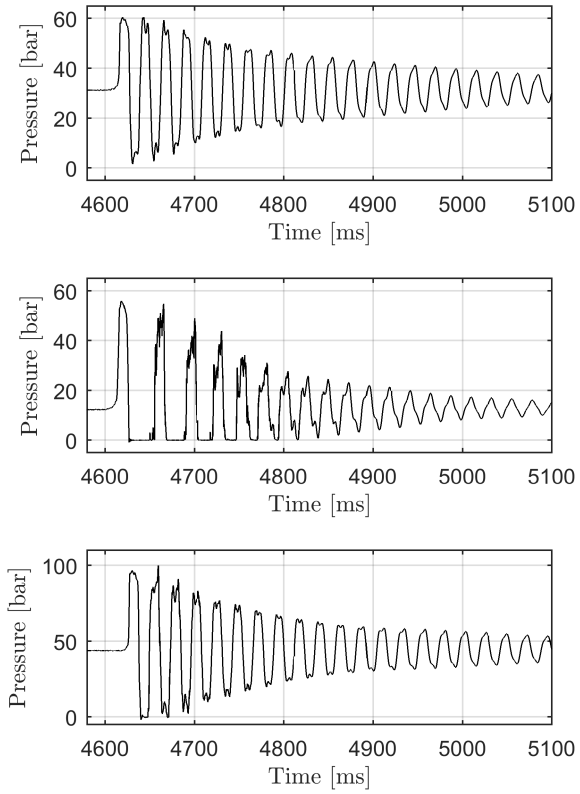

Fig. 6. Pressure trace of static pressure sensor 1 for case A (top), case B (middle) and case C (bottom)

is three times the first mode ($\lambda 3/4$ resonator). The notches in the pressure peaks can be considered as the 2nd mode. This observation is made for all peaks before $t = 4870$ ms except the first one. The Amplitude decreases over time, which is visible by comparing both FFTs.

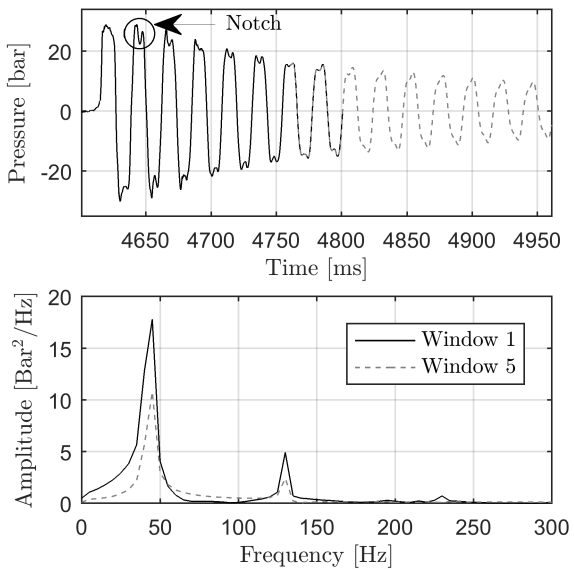

Fig. 7. Case A, sliding FFT, window 1 & 5: Pressure trace of the dynamic pressure sensor 1 (top), FFT for the shown pressure trace (bottom)

Case B

The equivalent plot to Fig. 7 for case B is shown in Fig. 8. The main difference to case A is the occurrence of cavitation. Since the pressure trace is not an harmonic oscillating signal, no clear peaks in the FFT are visible in window 1. A very broad peak in the range of $f = 0 - 100$ Hz is visible. This can be explained by the smaller frequency due to cavitation. As in case A, no 2nd mode is visible in the very first peak. In window 5 the FFT looks like the FFTs in case A. The pressure trace of window 5 looks different than the pressure trace in window 5 of case A. With respect to Eqs. 5 and 6 the shift in time is of interest. The first mode is used as the reference, therefore $\phi_1 = 0$. Because the wave troughs of M_2 are not in center of the peaks of M_1, $\phi_2 \neq 0$.

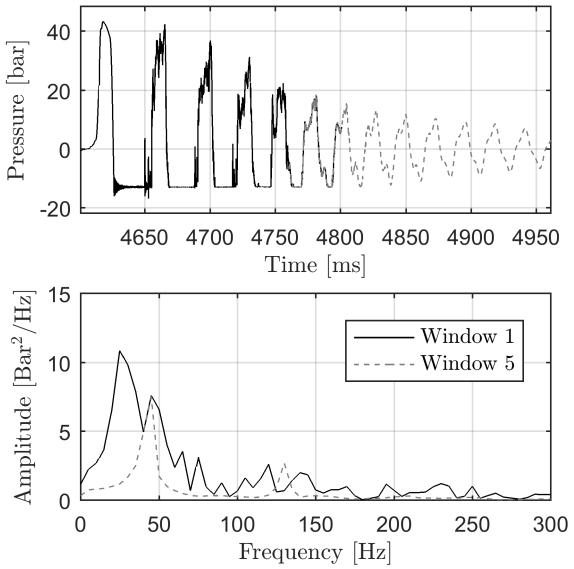

Fig. 8. Case B, sliding FFT, window 1 & 5: Pressure trace of the dynamic pressure sensor 1 (top), FFT for the shown pressure trace (bottom)

Case C

Fig. 9 is equal to Figs. 7 and 8. Occurrence of cavitation is visible in the first two valleys. In the first peak there is no notch is visible. This can be explained by the theory of the first peak being a pressure wave, which induces the pressure oscillation after it is reflected at the transition from pipeline to tank. The second peak is higher than the first one ($\Delta P_2 > \Delta P_1$). A possible explanation is beat coupling. After the area with cavitation the pressure trace is very similar to case A. Both FFTs are very similar to case A. The only difference is a peak around $f = 5$ Hz in the first window FFT.

4.4. Signal deconstruction

As shown in section **4.3.** the first two modes are the dominating oscillations in this section. These modes are isolated by a bandpass filter.[16] The input parameters of the bandpass filter are given in table 2.

Table 2. Input parameter of the bandpass filter.

Mode	Frequency f [Hz]	Filter frequency f_{BP} [Hz]
1	45	35 – 50
2	130	120 – 140

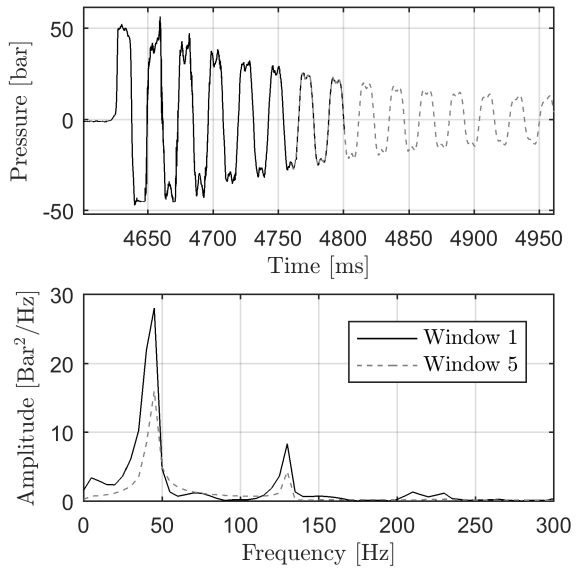

Fig. 9. Case C, sliding FFT, window 1 & 5: Pressure trace of the dynamic pressure sensor 1 (top), fft for the shown pressure trace (bottom)

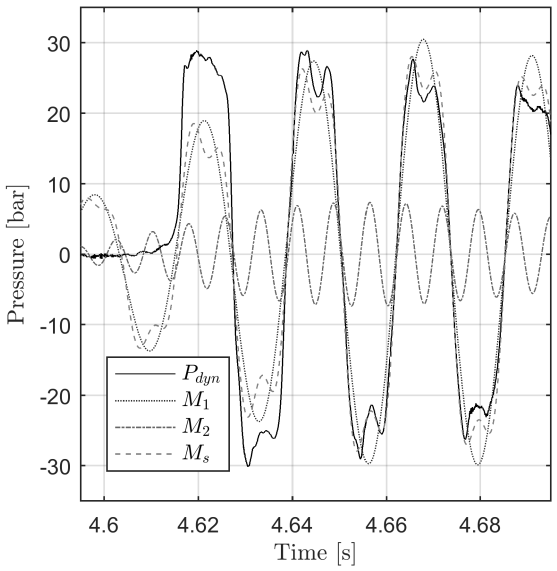

Fig. 10. Case A: Pressure trace from the dynamic pressure sensor 1 (P_{dyn}), filtered first mode M_1, filtered second mode M_2 and the summation of both modes $M_s = M_1 + M_2$

Case A

In Fig. 10 the first mode M_1, the second mode M_2, the summation of them $M_s = M_1 + M_2$ and the accompanying pressure signal P_{dyn} are shown. The legend used in Fig. 10 is used in Figs. 11 - 15.

Since the filter only works properly with periodic signals the filtered modes do not match the pressure trace before the first period is over (t = 4640 ms). They are shown to identify the point in time when a good overlay is present. After that point in time there is a good match between M_s and P_{dyn}.

In section **4.3.** the notches in the peaks were considered as the 2nd mode. By comparing M_1 and P_{dyn} it can be seen that the first mode is like the pressure trace but without the notches in the wave crests and troughs. Since M_s is matching well with P_{dyn} after t = 4640 ms and the only difference between M_1 and M_s is M_2, it is proven that the notches are the second mode.

A later time range of Fig. 10 is shown in Fig. 11. M_s matches will with P_{dyn} all the time. The notch from the overtone is in center of the peak and is shifted slightly to the left with increasing time.

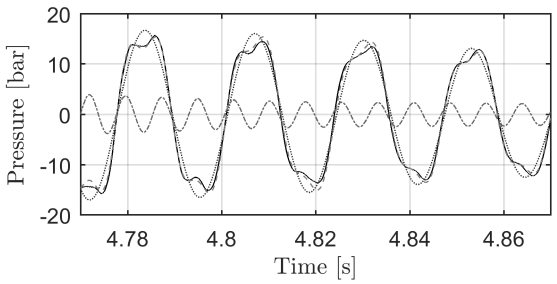

Fig. 11. Case A: Reconstructing pressure trace, legend can be found in Fig. 10

Case B

It is not possible to rebuild the signal while the occurrence of cavitation, since it is not periodic. This is visible in Fig. 12. Like in case A ,no overtones are visible in the first peak. An oscillation at f = 2530 Hz is observed in the first valley, a more detailed investigation will follow in future works. Several spikes are visible in the second peak. The source for these spikes is unclear but they appear as well in the following peaks. The pressure trace is more rough in a case with cavitation then without.

Fig. 13 shows a later time range for case B. The time frame starts at t = 4770 ms.The first peak in Fig. 13 is the last peak before the last wave trough with cavitation. M_s does not match well with the peak at t = 4780 ms in Fig. 13 which can be explained with the non periodic signal before t = 4770 ms.

Cavitation occurs in the valley at t = 4790 ms, P_{dyn} is dropping below the vapor pressure. This can be seen on the hori-

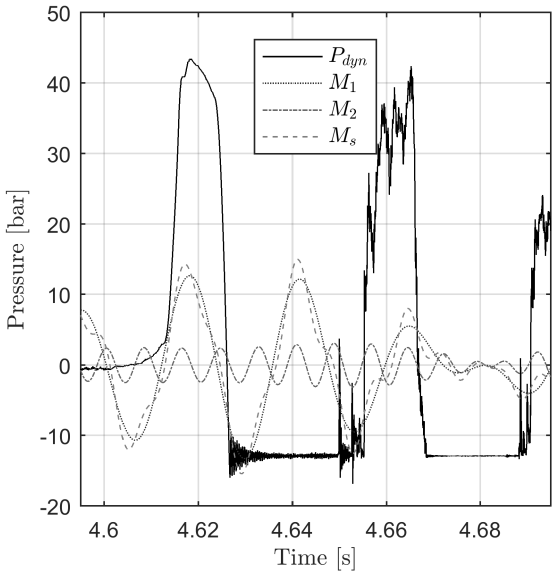

Fig. 12. Case B: Pressure trace from the dynamic pressure sensor 1 (P_{dyn}), filtered first mode M_1, filtered second mode M_2 and the summation of both modes $M_s = M_1 + M_2$

zontal line at $P_{dyn} = -12.9$ bar. With respect to M_1 the time of cavitation should be longer if there would be no overtones. It can be seen that the first mode is below the vapour pressure while the pressure signal is lifted above it by the second mode. Therefore it is assumed that the 2nd mode is excited even at the occurrence of cavitation.

After $t = 4800$ ms P_{dyn} and M_s matches very well. As in Fig. 11 the 2nd mode is slightly shifted to the left. The amplitude of the 2nd mode is relative to the first mode higher than in case A.

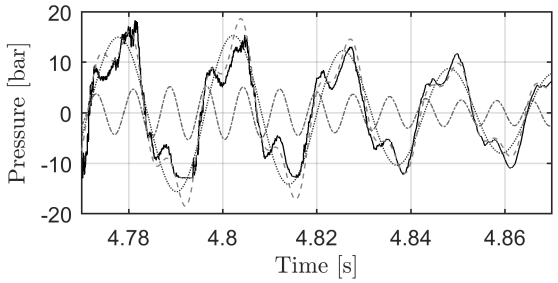

Fig. 13. Case B: Reconstructing pressure trace, legend can be found in Fig. 12

Case C

Case C is the link between case A and case B. Like in these cases no overtones are visible in the first peak. Fig. 14 is equal to Fig. 10. As expected the reconstruction of the signal using M_s does not work at the first period. P_{dyn} and M_s matches well after the second peak.

Cavitation occurs only in the first two valleys. By comparing M_s and M_1 to P_{dyn} at the second valley the same phenomenon as in case B is observed. The 2nd mode causes a pressure rise above the saturation pressure while the existence of cavitation. This observation proves that the 2nd mode is excited even at the occurrence of cavitation. It is not clear if this phenomenon occurs at the first valley. An overtone in the first wave trough of case A is visible (Fig. 10), therefore this behaviour may be suspected.

In comparison with case A and B the signal tends to get rougher with the occurrence of cavitation. A possible explanation is that the implosion of the cavitation leads to pressure waves which travel in the pipeline. With increasing time the amount of cavitation is decreasing and the induced pressure waves get damped. The pressure signal for all three cases is not rough after the cavitation disappears.

Fig. 15 is comparable to Figs. 11, 13. The pressure trace P_{dyn} and the modes M_1,M_2 are similar to case A. In case C the overtones notch is in the center of each peak. No shift between the modes can be observed, the reason for this behaviour is unclear. Since there is a shift for case A and B, it can not be reasoned in the occurrence of cavitation.

5. Damping

To determine the damping constant δ, static pressure sensor 1 is used. The damping of the modes M_1 and M_2 and the influence of cavitation on the damping is of interest. To ensure comparability a normalization for the pressrue signal is used. This normalization is like in[12] (Eq. 7). It creates an oscillation around 0 with a maximum of 1. Furthermore the data is cut

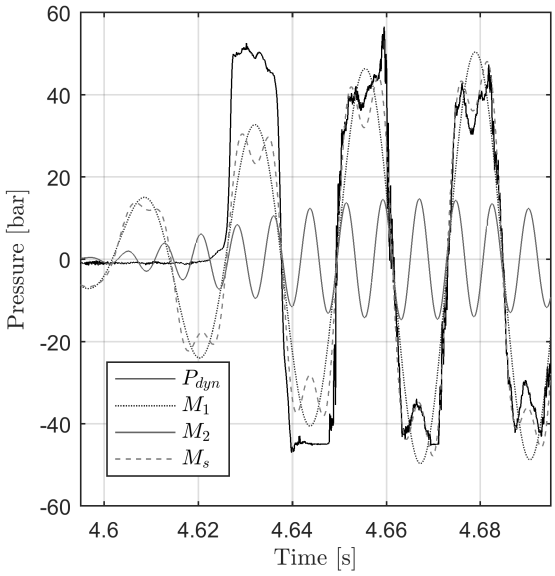

Fig. 14. Case C: Pressure trace from the dynamic pressure sensor 1 (P_{dyn}), filtered first mode M_1, filtered second mode M_2 and the summation of both modes $M_s = M_1 + M_2$

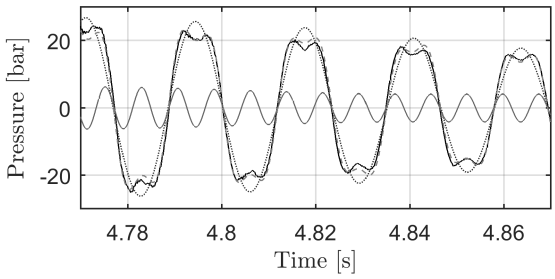

Fig. 15. Case C: Reconstructing pressure trace, legend can be found in Fig. 14

before the maximum peak.

$$P^*(t) = \frac{P(t) - P_{HP}}{P_{max} - P_{HP}} \tag{7}$$

First the damping constant δ is determined for all test cases. For 25 of 29 cases without cavitation the damping constants can be found in.[13] There δ was determined by using not normalized data. To determine δ an exponential function $y(t) = \hat{y}e^{-\delta * t}$ is fitted to the peaks of the normalized pressure trace.

The fit function for case A and B is plotted in Figs. 16, 17. In both cases a good agreement between the experimental determined peaks and the fit function is visible. Even the part where cavitation occurred is matching well. Therefore the exponential fit function $y(t) = \hat{y}e^{-\delta t}$ is considered to be a good way to determine and compare the damping constant δ. Due to normalization $\hat{y} \approx 1$.

5.1. Pressure trace damping

In this section the damping behaviour of all test cases, not only A,B and C is of interest.

The damping constant over the static pressure p_{HP} is plotted in Fig. 18. The trend for test cases without cavitation is a slight rise of δ for decreasing p_{HP}. One data point at $p_{HP} = 20$ bar shows a large deviation from this trend.

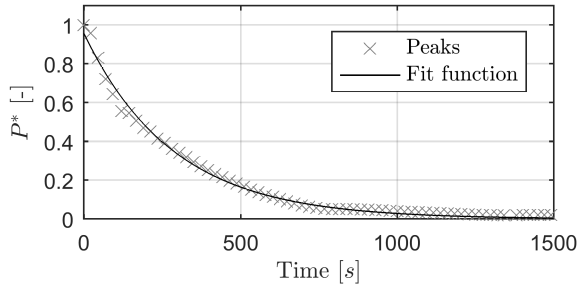

Fig. 16. Case A: Peaks of the pressure trace and the exponential fit function $y(t) = \hat{y}e^{-\delta t}$

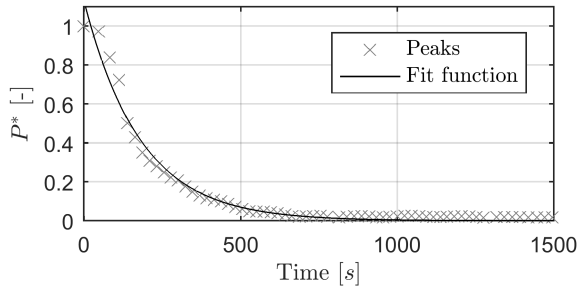

Fig. 17. Case B: Peaks of the pressure trace and the exponential fit function $y(t) = \hat{y}e^{-\delta t}$

For cases with cavitation the trend which is observed for cases without cavitation is the same for $p_{HP} < 20$ bar. Some outliers can be found for $p_{HP} \approx 2$ bar. For $p_{HP} = 20 - 25$ bar a very wide range of δ is observed. The reason is not clear and will be investigate in future works.

A few outliers can be spotted for $p_{HP} \approx 20$ bar. For cases with cavitation in comparison to no cavitation tests at the same p_{HP}, a slightly higher δ is observed.

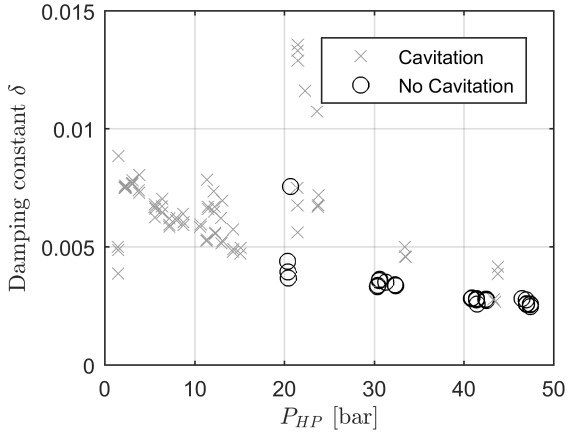

Fig. 18. Damping constant of the whole pressure signal δ over the static pressure P_{HP}.

In Fig. 19 δ is plot over the relative amplitude $\Delta P_1/P_{HP}$. Cavitation occurs only if $\Delta P_1/P_{HP} > 2$. No dependency on the relative amplitude can be found for δ but an increase can be seen for cases with cavitation. For these cases δ is nearly constant, with the exception of some outliers.

To isolate the influence from the cavitation only the harmonic oscillation of all test cases is investigated. To determine the damping constant of the harmonic oscillation δ_h the pressure signal is cut at the last wave trough with cavitation. As for the

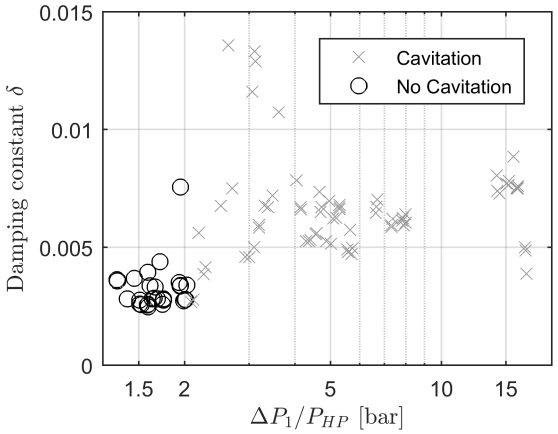

Fig. 19. Damping constant of the whole pressure signal δ over the relative amplitude $\Delta P_1/P_{HP}$.

determination of δ an exponential fit function $y(t) = \hat{y}e^{-\delta_h t}$ is used. The pressure peaks are the highest at the beginning. These peaks have an enormous effect on the damping constant, since they are missing for tests with cavitation for δ_h it is assumed that δ is more accurate than δ_h.

For cases without the occurrence of cavitation the whole signal is an harmonic oscillation, therefore $\delta = \delta_h$ in these cases.

In Fig. 20 the damping constant of the harmonic part δ_h is plot over P_{HP}. The results for $delta_h$ are in the same order of magnitude as δ (Fig. 18). The damping constant for cases with cavitation δ_h seems to be smaller than δ.

For $P_{HP} = 0 - 5$ bar the dispersion is very large. As shown in Fig. 5 these cases show a very high relative amplitude at around $P_{max}/P_{HP} \approx 15$. This high relative amplitude in combination with the low static pressure leads to a very low amplitude after the time interval with cavitation. For such small amplitudes the fit function is very vulnerable for deviations. This behaviour explains to big deviations for δ_h for cases with $P_{HP} < 5$ bar.

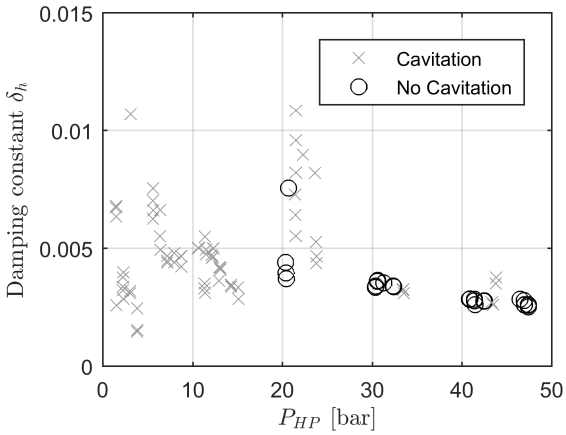

Fig. 20. Damping constant of the harmonic oscillation δ_h over the static pressure P_{HP}.

In Fig. 20 the damping constant of the harmonic part δ_h is plotted over the relative amplitude $\Delta P_1/P_{HP}$. The step of δ at the cavitation line ($\Delta P_1/P_{HP} > 2$) is not visible. Therefore it is assumed that the occurrence of cavitation leads to a shift of the damping constant. Systems with cavitation are more damped than systems without cavitation. The effect is in the same order

of magnitude then the pressure dependency of δ. The bigger deviation for δ_h then δ can be explained by released dissolved gas after the occurrence of cavitation which affects the damping behaviour of the system. Furthermore cavitation leads to more macroscopic movement and therefore more friction in the system.

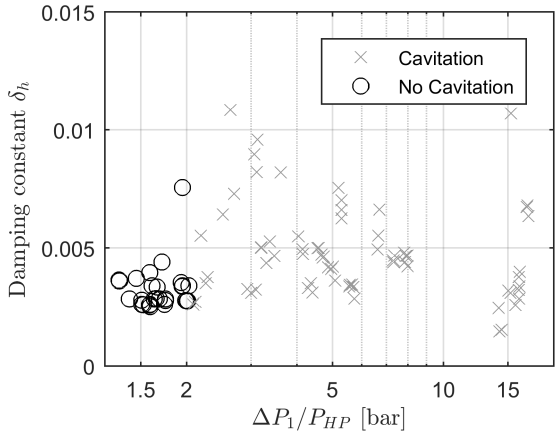

Fig. 21. Damping constant of the harmonic oscillation δ_h over the relative amplitude $\Delta P_1/P_{HP}$.

5.2. Mode damping

In Figs. 16, 17 deviations from the exponential fit and the peaks are visible. As shown in section **4.4.** it is possible to reconstruct the pressure signal P_{dyn} very precise with the first two modes M_1 and M_2 after the time range with cavitation. To get a more detailed understanding the damping constant of mode M_1 (δ_1, Fig. 22) and M_2 (δ_2, 24)) are calculated.

Since it is only possible to reconstruct the modes for an harmonic oscillation δ_1 and δ_2 are determined after the local maximum of M_1, respectively M_2 after the last wave trough with the occurrence of cavitation. To assure comparability between δ, δ_h and δ_1, δ_2 an exponential fit function $y(t) = \hat{y}e^{-\delta_{1,2}t}$ is used

Due to technical difficulties it was not possible to fit an exponential function on the first mode M_1 on 9 of 100 test cases, these tests are not shown in Figs. 22, 23.

In Fig. 22 the damping constants δ_1 is shown over p_{HP}. For cases without cavitation δ_1 is very similar to δ (Fig. 18. This can be explained by the first mode M_1 being the main part of the pressure signal. For cases with cavitation the damping constant δ_1 tend to be a bit lower than δ but is in the same order of magnitude. The trend from Fig. 18 can be observed in Fig. 22 but only for $P_{HP} > 10$ bar. This observation matches with the behaviour of δ as a function of p_{HP} for testcases without cavitation.[13)]

Since only the part after cavitation is considered for δ_1 this behaviour can be traced back to a possible pressure dependency of δ_1.

In the area of $p = 0 - 10$ bar the dispersion of δ is extremely high, this is comparable to δ_h. The lowest and highest δ_1 can be found here. As shown in Fig. 5 these tests got a very high relative amplitude, which indicates a lot of cavitation.

The damping constant δ_1 over the $\Delta P_1/P_{HP}$ is shown in Fig. 23. Large deviations occur for $\Delta P_1/P_{HP} > 5$ bar. This supports the statement that released dissolved gas after the occurrence of cavitation affects the damping behaviour of the system in a not predictable way.

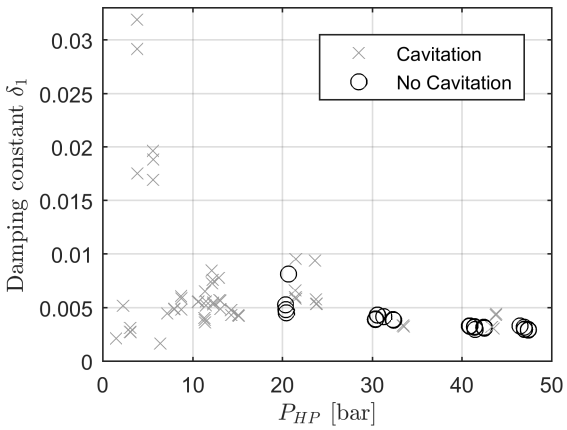

Fig. 22. Mode1: Damping constant δ_1 over the static pressure P_{HP}.

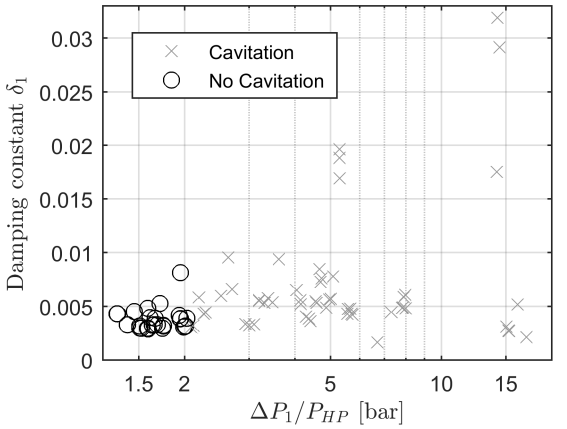

Fig. 23. Mode1: Damping constant δ_1 over the relative amplitude $\Delta P_1/P_{HP}$.

Due to technical difficulties it was not possible to fit an exponential function on the second mode M_2 on 15 of 100 test cases, these test cases are not shown in Figs. 24, 25. It was not possible to fit an e-function either on the first, nor the second mode in four test cases.

The damping constant of the second mode δ_2 is shown over p_{HP} in Fig. 24 and over $\Delta P_1/P_{HP}$ in Fig. 25. For $P_{HP} > 30$ δ_2 is higher than δ_1 and δ, thus M_2 is more damped than M_1. The dispersion is very high for $P_{HP} < 30$ bar, no dependency can be identified.

In Fig. 25 no trend of δ_2 in dependence of the relative amplitude can be observed. Most cases without cavitation show a uniform δ_2. The strong dispersion for tests with cavitation in Figs. 24, 25 may be explained by the low amplitude and strong damping. For a lot of cavitation, which can be achieved by a large relative amplitude, the amplitude of M_2 is very low at the beginning of the harmonic oscillation. Therefore test cases without cavitation can be trusted more to determine δ_2.

6. Conclusion and Outlook

To investigate the influence of cavitation on the damping constant one hundred water hammer tests have been performed at the test bench FTTF at DLR Lampoldshausen. The tests were

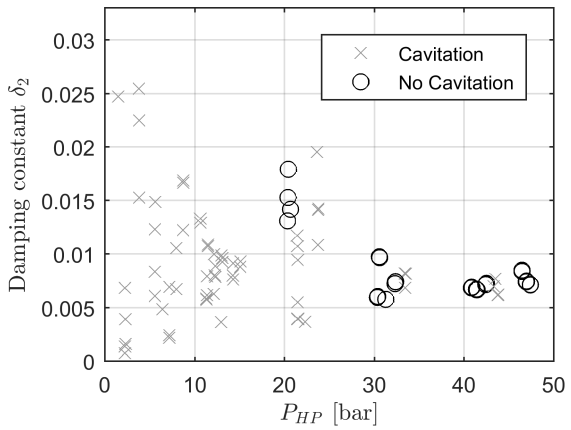

Fig. 24. Mode2: Damping constant δ_2 over the static pressure P_{HP}.

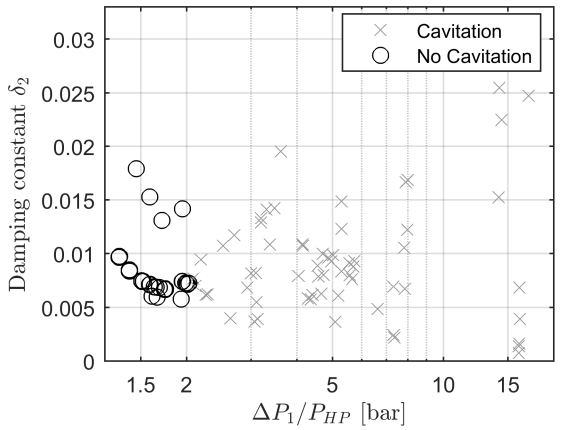

Fig. 25. Mode2: Damping constant δ_2 over the relative amplitude $\Delta P_1/P_{HP}$.

in a static pressure range from $1-50$ bar, where the relative amplitude goes up to 15. Cavitation occurred in $71/100$ tests, the amount of cavitation is in a very wide range. In some cases cavitation occurred only in the first wave trough, in others cavitation occurred in multiply wave troughs.

Three test cases (case A,B,C) were shown in detail. Case A did not include cavitation, case B includes cavitation in multiply wave troughs. Case C is the connection between case A and B, cavitation occurs only in the first two wave troughs.

An FFT was used to extract the frequency of the first two modes. It was shown that these frequencies are constant over time,but the second mode is shifted in time in comparison to the first mode. This behaviour was observed in case B.

By using a bandpass filter around the frequencies of the first two modes, the signal was deconstructed. It is possible to rebuild the signal by adding both modes. With these techniques it was possible to show that the second mode starts oscillating after the first wave crest and is oscillating even in the area of cavitation.

The damping constants for all test cases is determined by using an exponential fit function $y(t) = \hat{y}e^{\delta t}$. Multiple damping constants have been determined. The overall damping constant δ is determined by using the whole pressure signal. The damping constant δ_h is determined by using the pressure signal after cutting it at the last wave trough with cavitation. Here only the harmonic oscillation is used for the determination of δ_h. By using the modes $M_{1,2}$ the damping constants $\delta_{1,2}$ are determined. Since the modes show good matching with the experimental data after one oscillation and if there is no cavitation, the mode signal is cut one wavelength after the last wave trough with the occurrence of cavitation. The predicted pressure dependency of δ was observed. For $P_{HP} = 20$ bar a wide dispersion is observed. There was also a rise in δ for cases with cavitation identified. This rise is not visible in δ_h. Therefore it is assumed that this rise is due to the occurrence of cavitation.

It is shown that the second mode is stronger damped then the first one. Best reference cases are the tests without the occurrence of cavitation. The scattering of δ_1,δ_2 and δ_h is increasing with an increasing relative amplitude.

In future works the outliers of δ at $P_{HP} = 20$ bar will be investigated in detail. Furthermore the tests will be repeated with liquid nitrogen and liquid oxygen to compare fluids at ambient temperature to cryogenic fluids. Since liquid oxygen is the real fluid of rocket engine feed line systems, this is of great interest. One part of the cryogenic investigation will be the comparison of the damping constants.

It is interesting to compare these experimental observations with numerical models. Most friction models do not include a pressure term, therefore an adaptation of these observations could be of interest.

Acknowledgments

The authors greatly acknowledge the support of the DLR M3 test facility team during the construction and operation of the test bench. Furthermore Markus Ekert is thanked for his supporting work.

References

1) L'Hullier, V.: *Propulsion in the ATV Spacecraft System - Lessons Learnt*, 45th AIAA/ASME/SAE/ASEE Joint Propulsion Conference & Exhibit, Denver,2009.
2) Walters, T. and Walker, J.: *Propellant line waterhammer analysis during staging*, 28th Joint Propulsion Conference and Exhibit, 1992.
3) Walters, T.: *Rocket Propellant Line Waterhammer Transients in a Variable-g Environment*, Forum on Unsteady Flow, 1990.
4) Lardier, C.: *The soviet manned lunar program N1-L3*, Acta Astronautica, **142**, 2018, pp.184-192.
5) Bergant, A., Simpson, A.R., Tijsseling A.S.: *Water hammer with column separation: A historical review*, Journal of Fluids and Structures, **22**, 2006, pp.135-171.
6) Ghidaoui, M., Ming, Z., McInnis, D., and Axworthy, D.: *A Review of Water Hammer Theory and Practice*, ASME, **58**, 2005, pp.49-76.
7) Bergant, A., Simpson, A. and Tijsseling, A.: *Water Hammer with Column Seperation: A Review of Research in the Twentieth Century*, School of Civil and Environmental Engineering, University of Adelaide, 2002.
8) Gibek, I., Maisonneuve, Y.: *Waterhammer Tests With Real Propellants*, 41st AIAA/ASME/SAE/ASEE Joint Propulsion Conference & Exhibit, 2005.
9) Gouriet, J.-B., Huertas-Martinez, A., Buchlin, J.-M., Vetrano, M.-R. and Steelant, J.: *Multiphase Fluid Hammer With Cryogenic Fluids*, 5th Space Propulsion, Roma, 2016.
10) Traudt, T., Bombardieri, C. and Manfletti, C.: *Influences on Water Hammer Wave Shape an Experimental Study*, 63. Deutscher Luft- und Raumfahrtkongress, Augsburg, 2014.
11) Traudt, T., Bombardieri, C. and Manfletti, C.: *High Speed Imaging of*

Water Hammer with Column Separation, 12th Pressure Surge Conference, Dublin, 2015.

12) Bombardieri, C.: *Experimental Investigation of the Filling Process in Evacuated Spacecraft Propulsion System Feedlines*, Ph.D. Thesis, RWTH Aachen University, 2018.

13) Klein, S., Traudt, T., Bombardieri, C. and Oschwald, M.: *Influence of static pressure on the damping of pressure waves in rocket engine feed lines*, 13th Pressure Surge Conference, Bordeaux, 2015.

14) Wylie, E.B. and Streeter V. L.: *Fluid transients*, New York, McGraw-Hill International Book Co., 1978.

15) Wilson, P. S. and Roy, R.A.: *An audible demonstration of the speed of sound in bubbly liquids*, American Journal of Physics, **76**, 2008, pp.975-981.

16) Copyright 2004-2012, The MathWorks, Inc., https://de.mathworks.com/help/matlab/ref/timeseries.idealfilter.html (accessed April 17, 2019).